

Optimization of ionic configurations in battery materials by quantum annealing

Tobias Binninger,^{1,2,*} Yin-Ying Ting,^{1,2} Piotr M. Kowalski,^{1,2} and Michael H. Eikerling^{1,2,3}

¹*Theory and Computation of Energy Materials (IEK-13), Institute of Energy and Climate Research, Forschungszentrum Jülich GmbH, 52425 Jülich, Germany*

²*Jülich Aachen Research Alliance JARA Energy & Center for Simulation and Data Science (CSD), 52425 Jülich, Germany*

³*Chair of Theory and Computation of Energy Materials, Faculty of Georesources and Materials Engineering, RWTH Aachen University, Intzestr. 5, 52072 Aachen, Germany*

Energy materials with disorder in site occupation are challenging for computational studies due to an exponential scaling of the configuration space. We herein present a grand-canonical optimization method that enables the use of quantum annealing (QA) for sampling the ionic ground state. The method relies on a Legendre transformation of the Coulomb energy cost function that strongly reduces the effective coupling strengths of the fully connected problem, which is essential for effectiveness of QA. The approach is expected to be applicable to a variety of materials optimization problems.

Modeling of ionic arrangements in multi-elements compounds represents a ubiquitous challenge for computational research in energy materials. Materials with mixed or partially occupied lattice sites are widely investigated for energy applications, e.g., doped semiconductors for electronics and photovoltaics applications [1–3], intercalation or high entropy materials for Li-ion batteries (LIBs) [4, 5], and ionic conductors for all-solid-state batteries (ASSBs) [6, 7]. While the configurational arrangement of elements can significantly affect the computed thermodynamic [8, 9], electronic [10], chemical [11], and ionic-transport parameters [12, 13], construction of reliable models of occupation disorder represents a major difficulty for simulations [14–19].

For a simulation cell comprising M sites, a fraction θ of which being occupied, the total number of possible configurations is given by (using Stirling’s formula)

$$\binom{M}{\theta M} \approx \left[\theta^{-\theta} (1-\theta)^{-(1-\theta)} \right]^M. \quad (1)$$

The exponential scaling of the configuration space with system size (M) precludes an efficient sampling of all possible configurations. For many computational problems, thermodynamically relevant low(est)-energy configurations must be computed to obtain meaningful predictions of material properties. Finding such model ionic distributions requires efficient, beyond random sampling algorithms. Common approaches include the methods of cluster expansion [14, 15, 17, 18] and special quasirandom structures [16, 19]. Alternatively, computational workflows employ stochastic Monte Carlo methods, such as simulated annealing or parallel tempering, with a surrogate energy model to identify a number of candidate ground-state configurations [20, 21]. The obtained models are used for accurate and computationally intensive simulations, usually based on density functional theory (DFT) (e.g., [21]). For typical simulation cells of LIB materials containing less than a hundred intercalation sites, the total number of ionic configurations is of the

order of 10^9 – 10^{15} and the Monte Carlo sampling significantly contributes to the overall runtime of the entire computational workflow. More efficient sampling methods are thus needed, for instance, to simulate the charging/discharging characteristics of LIB cathodes.

Quantum computing (QC) techniques provide new ways of solving exponentially scaling problems in materials science. Among these, quantum annealing (QA) is designed to solve large-scale classical optimization problems. Using this approach, a problem is mapped onto an Ising-type Hamiltonian [22, 23], which is then optimized by QA to provide the ground state. The underlying procedure consists of adiabatically tuning an initial transverse-field Hamiltonian to the target Hamiltonian, encoding the cost function of the optimization problem. Then, the quantum state of the multi-qubit system adiabatically converges to the ground state of the target Hamiltonian, corresponding to the global minimum of the cost function. With the emergence of commercially available hardware, such as the QA devices by D-Wave Systems Inc., such methods should be tested and deployed in materials science research. The efficiency of QA depends on finding a suitable encoding of a given optimization problem on the QA hardware [24, 25]. Due to limited connectivity of the qubit network topology, this is particularly challenging for problems represented by a fully connected interaction graph [26], generally termed ‘clique’.

QA has been already applied for conformational sampling of polymer mixtures [27] and materials design and optimization [28, 29]. Carnevali et al. [30] and Camino et al. [31] have employed D-Wave QA devices for optimizing the distribution of vacancies in a graphene sheet. In their approach, each site i of the graphene lattice was represented by a binary site occupation variable $x_i \in \{0, 1\}$, indicating whether respective site is occupied or vacant. The surrogate energy model which represented the cost function of the optimization problem accounted for the number of intact vs. broken chemical bonds, depending

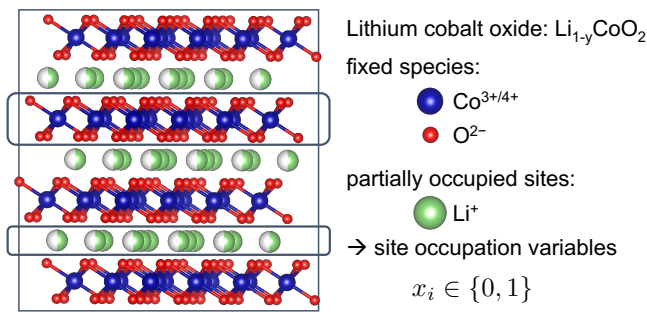
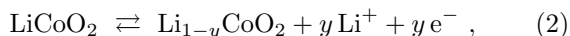


FIG. 1. Layered crystal structure of lithium cobalt oxide (LCO). Li sites are either vacant or occupied, resulting in many possible arrangements of Li ions across available sites.

on the distribution of vacancies. The limited number of chemical bonds per atom resulted in a limited number of non-zero $x_i x_j$ coupling terms in the cost function, which was beneficial for the mapping to the limited connectivity of the D-Wave qubit network topology. Optimization of the bare energy model naturally resulted in the complete occupation of all sites. In order to tune the system to a certain number of vacancies, an additional term of the form $(\sum_i x_i - N_C)^2$ was added to the cost function, penalizing any state with a total atom number different from the targeted value, N_C . However, this penalty term produces non-zero couplings of all pairs of variables, thus thwarting the beneficially sparse form of the bond energy model.

Herein, we demonstrate the use of quantum annealing for sampling the configurational ground state of ionic materials, employing the total Coulomb energy as a surrogate energy model. The long-range nature of Coulomb interactions couples any pair of lattice sites. The resulting full connectivity of the optimization problem is further exacerbated by the penalty term for the target stoichiometry constraint, making the problem extremely challenging for present-day QA architectures. To overcome this difficulty, we propose a grand-canonical sampling method employing a Legendre-transformed energy cost function that significantly alleviates the connectivity strength. The method renders the configurational optimization of LIB materials feasible on existing D-Wave QA hardware and has general applicability to similar problems in the research of disordered materials.

We have chosen lithium cobalt oxide (LCO), a standard cathode material for LIBs [32], as a test case. During charging/discharging of LCO, Li ions are extracted/intercalated according to the reaction:



resulting in the formation/filling of vacancies across the Li-ion sub-lattice. We target to model the semi-lithiated state with $\text{Li}_{0.5}\text{CoO}_2$ stoichiometry. The model cell, shown in Fig. 1, comprises 36 Li sites, half of which are occupied and half are vacant. The problem consists in

finding the ground-state configuration among the $\approx 10^{10}$ possible distributions of 18 Li ions over 36 available sites. The electrostatic Coulomb energy,

$$E_{\text{coul}} = \frac{e^2}{4\pi\epsilon_0} \sum_{\alpha < \beta} \frac{Z_\alpha Z_\beta}{|r_\alpha - r_\beta|} , \quad (3)$$

is the cost function to be minimized. Here, the summation goes over any pair of ions present in the structure, Z_α are the respective valencies, and other constants have their usual meaning. Standard valencies of $Z_{\text{Li}} = +1$ and $Z_{\text{O}} = -2$ have been chosen for lithium cations and oxygen anions, respectively, and $Z_{\text{Co}} = +3.5$, which is the (average) valency of cobalt cations in semi-lithiated LCO to provide overall charge neutrality. Assigning binary occupation variables x_i to each of the Li sites, indicating whether a given site is occupied ($x_i = 1$) or vacant ($x_i = 0$), the Coulomb energy can be written in terms of sums over all Li sites,

$$E_{\text{coul}} = \text{const} + \sum_{i \in S_{\text{Li}}} Q_{i,i} x_i + \sum_{i < j \in S_{\text{Li}}} Q_{i,j} x_i x_j . \quad (4)$$

Here, $\text{const} = \frac{e^2}{4\pi\epsilon_0} \sum_{i < j \in \text{fix}} \frac{Z_i Z_j}{|r_i - r_j|}$ is the Coulomb interaction energy among all fixed ions, i.e., cobalt cations and oxygen anions, and the coefficients $Q_{i,i} = \frac{e^2}{4\pi\epsilon_0} \sum_{j \in \text{fix}} \frac{Z_j}{|r_i - r_j|}$ and $Q_{i,j} = \frac{e^2}{4\pi\epsilon_0} \frac{1}{|r_i - r_j|}$ correspond to the Coulomb interaction between a given Li site i and fixed species, and between a given pair of Li sites, respectively. Due to the pairwise character of Coulomb interactions, Eq. (4) has the form of a quadratic unconstrained binary optimization (QUBO) problem, as required for present D-Wave QA devices.

For a periodic system, the QUBO coefficients $Q_{i,i}$ and $Q_{i,j}$ have to be computed in a way that correctly captures the long-range character of Coulomb interactions. To this end, we employed Ewald summation routines available in the `pymatgen` library [33] for `Python`. The constant term was obtained as the Ewald energy of the simulation cell with only fixed species present. To determine $Q_{i,i}$, simulation cells with only one occupied Li site i and all fixed ion species were constructed. The respective Ewald energies were corrected by subtracting the constant term to avoid over-counting of the interaction energy among fixed species. The coefficients $Q_{i,j}$ were obtained from the Ewald energies of simulation cells with only Li ions on sites i and j present (without any fixed ions). To avoid double counting, the respective energies were corrected for the self-energies of sites i and j , i.e., the interaction energy of Li ions on a single given site and all of its periodic images (which is already accounted for in the respective diagonal terms $Q_{i,i}$). We note that simulation cells comprising only a subset of ion species are not charge balanced. The Ewald method automatically adds a neutralizing homogeneous background charge to prevent divergence of the electrostatic energy. However, due

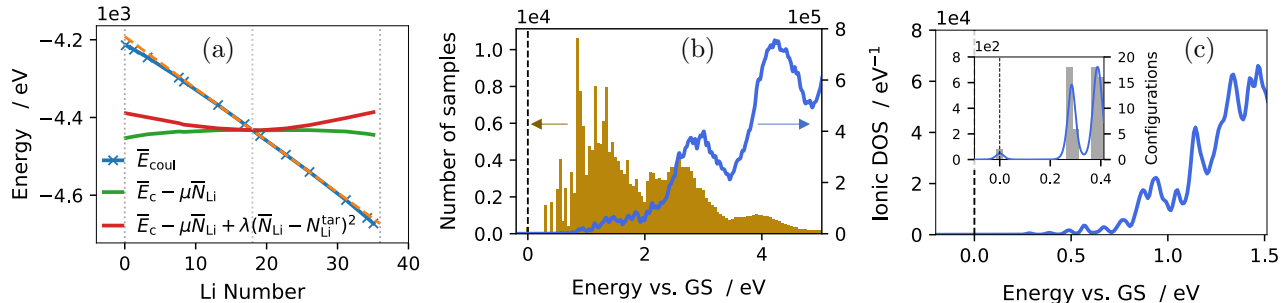


FIG. 2. (a) Average energy vs. Li number for LCO as obtained from the bare Coulomb energy model of Eq. (4) (blue curve with markers), after applying a Legendre transformation with $\mu = -13.38$ eV (green curve), and including the quadratic penalty term of Eq. (5) with $\lambda = 0.2$ (red curve). (b) Histogram of Coulomb energies obtained from QA with the grand-canonical method ($\mu = -13.2$ eV and $\lambda = 0.2$). Only samples with $N_{\text{Li}} = 18$ were counted. The energy is given vs. the ground-state (GS) energy ($E_{\text{coul}}^{\text{min}} = -4432.64$ eV). The ionic configurational density of states (DOS) of the Coulomb energy model, determined by REMC sampling, is shown for comparison (blue curve). (c) Ionic DOS, obtained from REMC sampling, in the energy range around the GS (blue: DOS curve with thermal broadening, left-hand axis; grey bars in inset: DOS histogram, right-hand axis).

TABLE I. Parameter tuning for sampling the ionic ground-state configuration of semi-lithiated LCO on a D-Wave Advantage™ system. For each set of parameters, 1000 independent annealing runs were performed with an annealing time of 100 μs each. λ : strength of Li number constraint; μ : chemical potential; \bar{N}_{Li} : average Li number; σ_c : chain strength; η_c : fraction of broken chains; $E_{\text{coul}}^{\text{min}}$: minimum value of Coulomb energy for configurations with target stoichiometry.

λ	μ	\bar{N}_{Li}	σ_c	η_c	$E_{\text{coul}}^{\text{min}}$
0	–	36	1	0.02%	–
0.5	–	34.9	1	49%	–
1.0	–	23.8	1	92%	–
1.0	–	24.3	5	0.03%	–
5.0	–	19.2	50	0.02%	–4427.08 eV
0.2	–13.2 eV	18.0	2	0.03%	–4432.64 eV

to charge neutrality of the overall system, background charge contributions mutually get cancelled and do not affect the total Coulomb energy of Eq. (4). The obtained QUBO coefficients for LCO were: $\text{const} = -4212.68$ eV, $Q_{i,i} = -9.40$ eV, and -1.04 eV $\leq Q_{i,j} \leq 2.02$ eV for $i < j$ ($Q_{i,j} = 0$ for $i > j$).

Having formulated the QUBO problem, we performed optimization of the obtained QUBO function using the D-Wave Advantage™ QA system. We note that due to pairwise Coulomb interactions the binary quadratic model is fully connected, i.e., all off-diagonal coefficients $Q_{i,j}$ ($i < j$) are non-zero. We thus employed the `DWaveCliquesampler()` routine from the D-Wave Ocean library. Minimization of the bare Coulomb energy cost function resulted in $x_i = 1$ for all 36 Li sites, i.e., complete occupation of the Li sublattice, as expected having strongly negative diagonal coefficients $Q_{i,i}$. To obtain the semi-lithiated state with desired occupation of

$N_{\text{Li}}^{\text{target}} = 18$ sites, the cost function must be modified to penalize configurations that violate the target stoichiometry. The standard approach to enforce such constraint consists in adding a following penalty term to the QUBO function [30, 31]:

$$\lambda \left(\sum_i x_i - N_{\text{Li}}^{\text{target}} \right)^2, \quad (5)$$

where $\sum_i x_i = N_{\text{Li}}$ is the total number of Li ions for a given configuration and λ is a parameter controlling the strength of the constraint term. Sampling statistics obtained for different values of λ are shown in Table I. With increasing λ , the average Li number \bar{N}_{Li} of the output configurations of 1000 independent annealing runs decreases towards the desired value of 18. However, at the same time the fraction of broken qubit chains [34], η_c , increases dramatically, from a negligible value for $\lambda = 0$ to 92% for $\lambda = 1$, rendering the solutions unreliable. This could be prevented by concomitantly increasing the chain strength parameter σ_c . For $\lambda = 5$ and $\sigma_c = 50$, we have achieved a negligible fraction of chain breaks and obtained the target stoichiometry of $N_{\text{Li}}^{\text{target}} = 18$ in 16% of annealing runs. The respective minimum value of the Coulomb energy is -4427.08 eV, which is still significantly larger than the minimum energy of -4432.64 eV obtained with classical replica exchange Monte Carlo (REMC) sampling. The reason for the poor performance of the QA method lies in the large value of $\lambda = 5$ required for the stoichiometry constraint, which adds a value of $2\lambda = 10$ to the off-diagonal elements of the coefficient matrix, a factor of 5–10 larger in magnitude than the off-diagonal contributions resulting from the Coulomb energy. In such a construction, thus, the stoichiometry constraint effectively masks the Coulomb energy terms and renders the optimization inefficient.

To meet the Li target stoichiometry at much smaller bias of the off-diagonal elements and improve the QA performance, we introduce a grand-canonical optimization method. Fig. 2a shows the average energy of sampled configurations as a function of the average Li number (blue curve with markers). A negative slope is apparent, explaining (i) why minimization of the bare energy resulted in maximum number of 36 Li ions and (ii) why a large value of λ is required in the quadratic penalty term to enforce a minimum of the cost function close to the target stoichiometry of 18. We interpret the slope as the chemical potential $\mu = \partial \bar{E}_{\text{coul}} / \partial \bar{N}_{\text{Li}}$ and rotate the energy curve by performing a Legendre transformation from Coulomb energy to the grand-canonical cost function $E_{\text{coul}} - \mu N_{\text{Li}}$. Using the fitted value of $\mu = -13.38$ eV (dashed line in Fig. 2a), the grand-canonical cost function becomes flat around the target stoichiometry with a slightly negative curvature (green curve in Fig. 2a) [35]. Having a so-transformed energy function, the quadratic penalty term of Eq. (5) with a small value of $\lambda = 0.2$ is then sufficient to bend the cost function upwards and produce a minimum at the target Li number (red curve in Fig. 2a). We note that the grand-canonical transformation only depends on the total Li number and therefore does not interfere with the energy optimization at the target stoichiometry. The total cost function for grand-canonical optimization thus reads

$$E_{\text{coul}}[\{x_i\}] - \mu \sum_{i \in S_{\text{Li}}} x_i + \lambda \left(\sum_{i \in S_{\text{Li}}} x_i - N_{\text{Li}}^{\text{target}} \right)^2, \quad (6)$$

where $E_{\text{coul}}[\{x_i\}]$ is given by Eq. (4).

Applying this method with a fine-tuned chemical potential of $\mu = -13.2$ eV, we obtained significantly better performance of the QA procedure, cf. Table I. The target stoichiometry of $N_{\text{Li}} = 18$ is met in 55% of returned configurations at a mild value of $\lambda = 0.2$. Most importantly, the minimum of returned Coulomb energies at the target stoichiometry is $E_{\text{coul}}^{\text{min}} = -4432.64$ eV, which is identical to the minimum energy obtained from the benchmark REMC sampling. The proposed grand-canonical method thus makes the fully connected Coulomb energy model feasible for optimization by QA, which is the main result of the present work.

To get better understanding of how QA works in practice, we performed a deeper analysis of the D-Wave sampling statistics. Fig. 2b presents a histogram of the Coulomb energies returned from 400'000 annealing runs (only counting energies of configurations with $N_{\text{Li}} = 18$). A broad distribution of energies is obtained, with most of the samples resulting in energies being few eV above the ground state (GS), whereas the true minimum energy solution was returned in only 0.083% of annealing runs. At first glance, this appears to be a rather low optimization efficiency. However, the configurational density of states (DOS) of the underlying model must be anal-

ysed for a fair assessment of the statistics [40]. The ionic configurational DOS of the Coulomb energy model was obtained from extended REMC sampling runs at parallel temperatures $kT = 0.05, 0.1, 0.2, 0.5, 1.0, 2.0, 5.0$ eV. It is shown as a blue curve in Fig. 2b, with close-ups around the GS energy in Fig. 2c. The essential structure of the QA sampling histogram (golden bars in Fig. 2b) reflects the shape of the underlying DOS. Assuming that each configuration is sampled with a certain “intrinsic” probability, $p(E)$, that only depends on the respective energy, the overall sampling rate, $N(E)$, is proportional to $p(E)$ times the number of states with energy E , i.e., the configurational DOS, $N_{\text{DOS}}(E)$,

$$N(E) \propto p(E) N_{\text{DOS}}(E). \quad (7)$$

In order to extract the intrinsic probability, $p(E)$, we normalized the QA sampling histogram with the configurational DOS. The result is shown in Fig. 3a. A monotonically decreasing sampling probability as a function of energy is obtained, clearly indicating that the lower energy configurations are sampled with higher probability, with the ground-state configuration having the highest sampling probability. As can be seen in Fig. 3a, the obtained $p(E)$ curve is well reproduced by a Boltzmann-type exponential function, $\exp(-E/kT)$, with a fitted value of $kT = 0.31$ eV (orange curve). Such a Boltzmann-type QA statistics has been observed previously [40–42]. It has been explained by statistical imperfections in tuning the target Hamiltonian during annealing runs [40]. We note that the *effective* sampling temperature depends on the problem at hand and is not related to the physical temperature of the hardware [41].

At first glance, our fitted value of $kT = 0.31$ eV indicates “hot” sampling of the configurational space. On the other hand, the effective temperature scales with the energy scale of the problem. The Coulomb energy of Eq. (4) considered by us represents a hard energy model, because it neglects dielectric screening. Including the latter in the form of a dielectric constant, ϵ_r , scales down all energies, and thus the effective sampling temperature. To estimate ϵ_r , we have computed the energies of 100 randomly selected ionic configurations at the density functional theory (DFT) level (cf. computational details in the caption of Fig. 3). Fig. 3b reveals a linear correlation between the Coulomb and corresponding DFT energies, which demonstrates the physical meaningfulness of the ionic Coulomb energy model for LCO. Since DFT energies implicitly include the effect of electronic screening, we interpret the slope of the plot in Fig. 3b as an effective dielectric constant, $\epsilon_r = 12$, which reduces the effective sampling temperature to $kT/\epsilon_r = 0.026$ eV, i.e., room-temperature.

In summary, we have presented here an efficient grand-canonical optimization method, which renders quantum annealing feasible for sampling the ionic ground state of battery materials based on a fully interacting

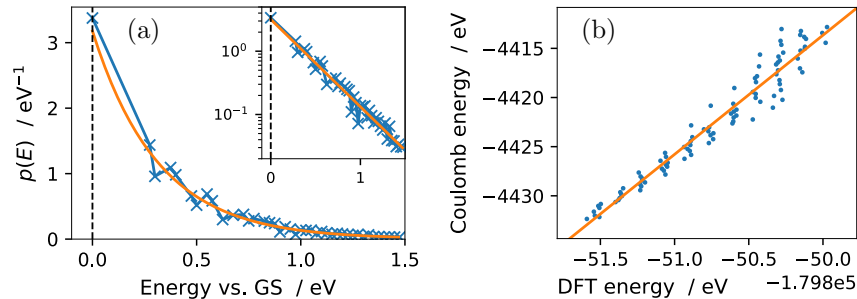


FIG. 3. (a) Intrinsic sampling probability (per energy), $p(E)$, obtained by dividing the overall sampling rate by the configurational DOS. The curve is well reproduced by a Boltzmann-type exponential decay $\exp(-E/kT)$ (orange fitted curve). The inset shows the same plot on a logarithmic scale. (b) Comparison of the Coulomb energy vs. DFT energy for 100 different ionic configurations of semi-lithiated LCO. DFT method: Calculations performed with Quantum Espresso software package [36]; Ultrasoft pseudopotentials [37] with GGA-PBEsol [38] exchange-correlation functional; DFT+ U method with Hubbard parameter $U = 4.6$ eV for cobalt [39]; Cutoff energy of 50 Ry for plane-wave basis set; $3 \times 4 \times 2$ k -point mesh.

Coulomb energy model. The method has been demonstrated on a D-Wave Advantage™ quantum annealer to successfully identify the lowest energy arrangement of lithium ions in lithium cobalt oxide. Boltzmann-type output statistics was observed with the highest sampling probability for the ground state configuration. We consider the grand-canonical optimization method to be of more general applicability to the solution of materials optimization problems by quantum computing.

The authors gratefully acknowledge the Jülich Supercomputing Centre (<https://www.fz-juelich.de/ias/jsc>) for funding this project by providing computing time on the D-Wave Advantage™ System JUPSI through the Jülich UNified Infrastructure for Quantum computing (JUNIQU). DFT simulations were performed on the JURECA machine in the scope of the project cjek13. The presented work was carried out within the framework of the Helmholtz Association’s program Materials and Technologies for the Energy Transition, Topic 2: Electrochemical Energy Storage.

* t.binninger@fz-juelich.de

- [1] S. Chen, A. Walsh, J.-H. Yang, X. G. Gong, L. Sun, P.-X. Yang, J.-H. Chu, and S.-H. Wei, Compositional dependence of structural and electronic properties of $\text{Cu}_2\text{ZnSn}(\text{S},\text{Se})_4$ alloys for thin film solar cells, *Phys. Rev. B* **83**, 125201 (2011).
- [2] S. Gu, R. Lin, Q. Han, Y. Gao, H. Tan, and J. Zhu, Tin and Mixed Lead–Tin Halide Perovskite Solar Cells: Progress and their Application in Tandem Solar Cells, *Advanced Materials* **32**, 1907392 (2020).
- [3] H. Helmers, E. Lopez, O. Höhn, D. Lackner, J. Schön, M. Schauerte, M. Schachtner, F. Dimroth, and A. W. Bett, 68.9% Efficient GaAs-Based Photonic Power Conversion Enabled by Photon Recycling and Optical Resonance, *physica status solidi (RRL) – Rapid Research Letters* **15**, 2100113 (2021).
- [4] T. Ohzuku and Y. Makimura, Layered Lithium Insertion Material of $\text{LiCo}_{1/3}\text{Ni}_{1/3}\text{Mn}_{1/3}\text{O}_2$ for Lithium-Ion Batteries, *Chem. Lett.* **30**, 642 (2001).
- [5] A. Sarkar, L. Velasco, D. Wang, Q. Wang, G. Talasila, L. de Biasi, C. Kübel, T. Brezesinski, S. S. Bhattacharya, H. Hahn, and B. Breitung, High entropy oxides for reversible energy storage, *Nat Commun* **9**, 3400 (2018).
- [6] R. Murugan, V. Thangadurai, and W. Weppner, Fast Lithium Ion Conduction in Garnet-Type $\text{Li}_7\text{La}_3\text{Zr}_2\text{O}_{12}$, *Angewandte Chemie International Edition* **46**, 7778 (2007).
- [7] D. Bérardan, S. Franger, A. K. Meena, and N. Dragoë, Room temperature lithium superionic conductivity in high entropy oxides, *J. Mater. Chem. A* **4**, 9536 (2016).
- [8] J. Liu, M. V. Fernández-Serra, and P. B. Allen, Special quasicrystalline structures: Role of short-range order in the semiconductor alloy $(\text{GaN})_{1-x}(\text{ZnO})_x$, *Phys. Rev. B* **93**, 054207 (2016).
- [9] S. Finkeldei, P. Kegler, P. Kowalski, C. Schreinemachers, F. Brandt, A. Bukaemskiy, V. Vinograd, G. Beridze, A. Shelyug, A. Navrotsky, and D. Bosbach, Composition dependent order-disorder transition in $\text{Nd}_x\text{Zr}_{1-x}\text{O}_{2-0.5x}$ pyrochlores: A combined structural, calorimetric and ab initio modeling study, *Acta Mater.* **125**, 166 (2017).
- [10] J. Yang, P. Zhang, and S.-H. Wei, Band Structure Engineering of $\text{Cs}_2\text{AgBiBr}_6$ Perovskite through Order–Disordered Transition: A First-Principle Study, *J. Phys. Chem. Lett.* **9**, 31 (2018).
- [11] S. Chae, L. Williams, J. Lee, J. T. Heron, and E. Kioupakis, Effects of local compositional and structural disorder on vacancy formation in entropy-stabilized oxides from first-principles, *npj Comput Mater* **8**, 1 (2022).
- [12] T. Connor, O. Cheong, T. Bornhake, A. C. Shad, R. Tesch, M. Sun, Z. He, A. Bukayemsky, V. L. Vinograd, S. C. Finkeldei, and P. M. Kowalski, Pyrochlore compounds from atomistic simulations, *Frontiers in Chemistry* **9**, 940 (2021).
- [13] A. A. Bukaemskiy, V. L. Vinograd, and P. M. Kowalski, Ion distribution models for defect fluorite $\text{ZrO}_2\text{-AO}_{1.5}$ ($A=\text{Ln}, \text{Y}$) solid solutions: I. relationship between lattice parameter and composition, *Acta Mater.* **202**, 99 (2021).

- [14] J. M. Sanchez, F. Ducastelle, and D. Gratias, Generalized cluster description of multicomponent systems, *Physica A: Statistical Mechanics and its Applications* **128**, 334 (1984).
- [15] D. B. Laks, L. G. Ferreira, S. Froyen, and A. Zunger, Efficient cluster expansion for substitutional systems, *Phys. Rev. B* **46**, 12587 (1992).
- [16] A. Zunger, S.-H. Wei, L. G. Ferreira, and J. E. Bernard, Special quasirandom structures, *Phys. Rev. Lett.* **65**, 353 (1990).
- [17] A. van de Walle, M. Asta, and G. Ceder, The alloy theoretic automated toolkit: A user guide, *Calphad* **26**, 539 (2002).
- [18] D. Lerch, O. Wieckhorst, G. L. W. Hart, R. W. Forcade, and S. Müller, UNCLE: A code for constructing cluster expansions for arbitrary lattices with minimal user-input, *Modelling Simul. Mater. Sci. Eng.* **17**, 055003 (2009).
- [19] K. Okhotnikov, T. Charpentier, and S. Cadars, Supercell program: A combinatorial structure-generation approach for the local-level modeling of atomic substitutions and partial occupancies in crystals, *Journal of Cheminformatics* **8**, 17 (2016).
- [20] M. Mottet, A. Marcolongo, T. Laino, and I. Tavernelli, Doping in garnet-type electrolytes: Kinetic and thermodynamic effects from molecular dynamics simulations, *Phys. Rev. Mater.* **3**, 035403 (2019).
- [21] T. Binninger, A. Marcolongo, M. Mottet, V. Weber, and T. Laino, Comparison of computational methods for the electrochemical stability window of solid-state electrolyte materials, *J. Mater. Chem. A* **8**, 1347 (2020).
- [22] P. Hauke, H. G. Katzgraber, W. Lechner, H. Nishimori, and W. D. Oliver, Perspectives of quantum annealing: Methods and implementations, *Rep. Prog. Phys.* **83**, 054401 (2020).
- [23] M. Jünger, E. Lobe, P. Mutzel, G. Reinelt, F. Rendl, G. Rinaldi, and T. Stollenwerk, Quantum Annealing versus Digital Computing: An Experimental Comparison, *ACM J. Exp. Algorithmics* **26**, 1.9:1 (2021).
- [24] N. Chancellor, Domain wall encoding of discrete variables for quantum annealing and QAOA, *Quantum Sci. Technol.* **4**, 045004 (2019).
- [25] J. Chen, T. Stollenwerk, and N. Chancellor, Performance of domain-wall encoding for quantum annealing, *IEEE Transactions on Quantum Engineering* **2**, 1 (2021).
- [26] E. Pelofske, G. Hahn, and H. N. Djidjev, Solving larger maximum clique problems using parallel quantum annealing, *Quantum Inf Process* **22**, 219 (2023).
- [27] C. Micheletti, P. Hauke, and P. Faccioli, Polymer Physics by Quantum Computing, *Phys. Rev. Lett.* **127**, 080501 (2021).
- [28] K. Kitai, J. Guo, S. Ju, S. Tanaka, K. Tsuda, J. Shiomi, and R. Tamura, Designing metamaterials with quantum annealing and factorization machines, *Phys. Rev. Res.* **2**, 013319 (2020).
- [29] K. Hatakeyama-Sato, T. Kashikawa, K. Kimura, and K. Oyaizu, Tackling the Challenge of a Huge Materials Science Search Space with Quantum-Inspired Annealing, *Advanced Intelligent Systems* **3**, 2000209 (2021).
- [30] V. Carnevali, I. Siloi, R. Di Felice, and M. Fornari, Vacancies in graphene: An application of adiabatic quantum optimization, *Phys. Chem. Chem. Phys.* **22**, 27332 (2020).
- [31] B. Camino, J. Buckeridge, P. A. Warburton, V. Kendon, and S. M. Woodley, Quantum computing and materials science: A practical guide to applying quantum annealing to the configurational analysis of materials, *Journal of Applied Physics* **133**, 221102 (2023).
- [32] K. Mizushima, P. C. Jones, P. J. Wiseman, and J. B. Goodenough, Li_xCoO_2 ($0 < x < -1$): A new cathode material for batteries of high energy density, *Materials Research Bulletin* **15**, 783 (1980).
- [33] S. P. Ong, W. D. Richards, A. Jain, G. Hautier, M. Kocher, S. Cholia, D. Gunter, V. L. Chevrier, K. A. Persson, and G. Ceder, Python Materials Genomics (pymatgen): A robust, open-source python library for materials analysis, *Computational Materials Science* **68**, 314 (2013).
- [34] The D-Wave Advantage™ system employs the so-called Pegasus topology of the qubit network with ≈ 15 connections per qubit. Depending on the connectivity of the QUBO problem, each logical variable must be represented by a group, or chain, of physical qubits. All qubits of a given chain must return the same value, which is achieved by tuning the respective coupling strengths via the chain strength parameter σ_c .
- [35] We consider the slightly negative curvature of the energy vs. Li number to result from the compensating background charge implicitly applied for systems with $N_{\text{Li}} \neq 18$. In contrast, in a real system, charge compensation upon lithiation/delithiation is provided by a reduction/oxidation of the redox-active transition metal (TM) ion species. The respective chemical hardness of TM ions introduces a positive energy curvature [43], as required for thermodynamic stability of the system.
- [36] P. Giannozzi, S. Baroni, N. Bonini, M. Calandra, R. Car, C. Cavazzoni, D. Ceresoli, G. L. Chiarotti, M. Cococcioni, I. Dabo, A. D. Corso, S. de Gironcoli, S. Fabris, G. Fratesi, R. Gebauer, U. Gerstmann, C. Gougoussis, A. Kokalj, M. Lazzeri, L. Martin-Samos, N. Marzari, F. Mauri, R. Mazzarello, S. Paolini, A. Pasquarello, L. Paulatto, C. Sbraccia, S. Scandolo, G. Sclauzero, A. P. Seitsonen, A. Smogunov, P. Umari, and R. M. Wentzcovitch, QUANTUM ESPRESSO: A modular and open-source software project for quantum simulations of materials, *J. Phys.: Condens. Matter* **21**, 395502 (2009).
- [37] D. Vanderbilt, Soft self-consistent pseudopotentials in a generalized eigenvalue formalism, *Phys. Rev. B* **41**, 7892 (1990).
- [38] J. P. Perdew, A. Ruzsinszky, G. I. Csonka, O. A. Vydrov, G. E. Scuseria, L. A. Constantin, X. Zhou, and K. Burke, Restoring the Density-Gradient Expansion for Exchange in Solids and Surfaces, *Phys. Rev. Lett.* **100**, 136406 (2008).
- [39] Y.-Y. Ting and P. M. Kowalski, Refined dft+*u* method for computation of layered oxide cathode materials, *Electrochimica Acta* **443**, 141912 (2023).
- [40] J. Brugger, C. Seidel, M. Streif, F. A. Wudarski, C. Dittel, and A. Buchleitner, Output statistics of quantum annealers with disorder, *Phys. Rev. A* **105**, 042605 (2022).
- [41] M. Benedetti, J. Realpe-Gómez, R. Biswas, and A. Perdomo-Ortiz, Estimation of effective temperatures in quantum annealers for sampling applications: A case study with possible applications in deep learning, *Phys. Rev. A* **94**, 022308 (2016).
- [42] M. Benedetti, J. Realpe-Gómez, R. Biswas, and A. Perdomo-Ortiz, Quantum-Assisted Learning of Hardware-Embedded Probabilistic Graphical Models, *Phys. Rev. X* **7**, 041052 (2017).

- [43] M. Saubanère, M. B. Yahia, S. Lebègue, and M.-L. Doublet, An intuitive and efficient method for cell voltage prediction of lithium and sodium-ion batteries, *Nat Commun* **5**, 5559 (2014).